PCCP

RSC Publishing

PAPER

Pt based PEMFC catalysts prepared from colloidal particle suspensions – a toolbox for model studies†

Cite this: *Phys. Chem. Chem. Phys.*, 2013, **15**, 3602

Jozsef Speder,[a] Lena Altmann,[b] Melanie Roefzaad,[a] Marcus Bäumer,[b] Jacob J. K. Kirkensgaard,[c] Kell Mortensen[c] and Matthias Arenz*[a]

Received 17th December 2012,
Accepted 17th January 2013

DOI: 10.1039/c3cp50195g

www.rsc.org/pccp

A colloidal synthesis approach is presented that allows systematic studies of the properties of supported proton exchange membrane fuel cell (PEMFC) catalysts. The applied synthesis route is based on the preparation of monodisperse nanoparticles in the absence of strong binding organic stabilizing agents. No temperature post-treatment of the catalyst is required rendering the synthesis route ideally suitable for comparative studies. We report work concerning a series of catalysts based on the same colloidal Pt nanoparticle (NP) suspension, but with different high surface area (HSA) carbon supports. It is shown that for the prepared catalysts the carbon support has no catalytic co-function, but carbon pre-treatment leads to enhanced sticking of the Pt NPs on the support. An unwanted side effect, however, is NP agglomeration during synthesis. By contrast, enhanced NP sticking without agglomeration can be accomplished by the addition of an ionomer to the NP suspension. The catalytic activity of the prepared catalysts for the oxygen reduction reaction is comparable to industrial catalysts and no influence of the particle size is found in the range of 2–5 nm.

1 Introduction

Low temperature proton exchange membrane fuel cells (PEMFCs) are widely considered as future means to clean and efficiently convert chemical into electric energy. In the last decade, research concerned with enhancing the activity of PEMFC catalysts has resulted in impressive improvements – both for precious metal and non-precious metal based catalysts.[1–5]

In order to transfer this knowledge to industrial catalysts and make use of the full catalyst potential demonstrated in model studies, systematic investigations on supported catalysts are essential. The synthesis routes traditionally used for the preparation of precious metal based, supported PEMFC catalysts such as impregnation or precipitation, however, offer only a limited control over the structure of the active component (typically Pt or Pt-alloy nanoparticles) and the support properties. Although active and efficient catalysts can be prepared following these routes, the synthesis is widely based on a ''try and error'' approach and many studies with contradicting results can be found in the literature. One of the reasons for these contradicting results is that often catalysts were prepared by different synthesis routes, making a direct comparison difficult.[6] The limited flexibility of traditional synthesis routes inhibits systematic studies and especially the role of the substrate often is difficult to assess. For example, our group reported recently a study on the degradation mechanism of different carbon supported Pt catalysts (Pt/C) applying identical location transmission electron microscopy (IL-TEM),[7] where it was shown that essentially each of the studied, commercially synthesized catalysts behaved differently.[8] No simple correlation between properties such as Pt particle size or the support and the degradation channel was found. Moreover, recently it was even shown that on the same Pt/C catalyst several different degradation mechanisms can be observed in areas of close proximity.[9] All these examples demonstrate the considerable inhomogeneity of supported catalysts studied. This inhomogeneity may be caused by the synthesis procedure, but also by the catalyst support.

In the following, we demonstrate how a colloidal synthesis approach can be used to systematically study the properties of PEMFC catalysts. The applied synthesis route allows the preparation of monodisperse nanoparticles (NPs) in the absence of strong binding organic stabilizing agents; the NP solution contains only ethylene glycol (EG) as an organic reagent, which is removed by washing with HCl before attaching the NPs to the support. No temperature post-treatment of the catalyst is required,

[a] *Nano-Science Center, Department of Chemistry, University of Copenhagen, Universitetsparken 5, DK-2100 Copenhagen Ø, Denmark. E-mail: m.arenz@chem.ku.dk*
[b] *Institute of Applied and Physical Chemistry, University of Bremen, Germany*
[c] *Niels Bohr Institute, University of Copenhagen, Denmark*

† Electronic supplementary information (ESI) available. See DOI: 10.1039/c3cp50195g

rendering the approach ideally suitable for such studies. By preparing a series of catalysts based on the same colloidal Pt NP solution but with different high surface area (HSA) carbon supports, we demonstrate that in contrast to some reports[10–12] the carbon support has no catalytic co-function and a carbon pre-treatment leads to enhanced sticking of the Pt NPs on the support, but can also result in enhanced NP agglomeration. Furthermore, we demonstrate that the ionomer addition to the catalyst ink typically used for preparing membrane electrode assemblies can be incorporated into the catalyst synthesis leading to an optimized electrochemically accessible Pt surface area (ECSA) of the catalyst.

2 Experimental

The synthesis of the electrocatalysts consists of two main steps. First, a solution of colloidal Pt NPs with narrow size distribution is prepared *via* an EG route. Then the NPs are precipitated from the EG-solution and resolved in acetone prior to deposition onto the HSA carbon support.

2.1 Nanoparticle synthesis

A detailed description of the Pt NP preparation method can be found in ref. 13. Briefly, a colloidal suspension of Pt NPs is synthesized by mixing under vigorous stirring 50 ml of a 0.4 M NaOH/ethylene glycol solution with a solution of 1.0 g $H_2PtCl_6{\cdot}xH_2O$ dissolved in 50 ml ethylene glycol, in order to obtain a yellowish platinum hydroxide or oxide colloidal solution. The colloidal solution is then heated to 160 °C for 3 h to obtain a blackish-brown homogeneous metal particle colloidal suspension. The size and structure of the thus synthesized Pt NPs are controlled by transmission electron microscopy (TEM). The average diameter of the obtained Pt NPs is typically around 1.5 nm exhibiting a narrow size distribution.

2.2 Preparation supported nanoparticles

In order to support the Pt NPs onto a HSA carbon first 40 ml of HCl was added to the colloidal NP solution for precipitation. The solution was centrifuged (4000 rpm, 6 min) and repeatedly washed with 1 M HCl before dispersing it in acetone. The as-synthesized Pt NPs were deposited onto different HSA carbons by mixing the NP suspension with carbon black in 3 ml of acetone and sonicating for 1 h. Finally the catalyst was dried.

2.3 High surface area carbon supports

As support materials different HSA carbon supports were employed: as-received EC300 Ketjenblack (AkzoNobel, BET area: 795 $m^2\ g^{-1}$) and graphitized Ruβ (BET area: 135 $m^2\ g^{-1}$) as well as EC300 Ketjenblack treated according to the following procedures.

As EC300-HNO_3 we denote Ketjenblack that was boiled under reflux at 80 °C for 8 h in 70% HNO_3 in order to introduce surface oxides,[14] followed by washing with distilled water and drying in an oven at 75 °C.

As EC300-PA (polyaniline) and EC300-CoED we denote Ketjenblack that was nitrogen-doped using either aniline or ethylenediamine (ED) according to ref. 15 and 16; *i.e.* 0.1 g EC300-HNO_3 carbon was ultrasonically dispersed in a mixture of 40 ml of 1 M HCl solution and 0.2 ml of aniline. The polymerization of the aniline was initiated by adding drop wise 0.5 g of ammonium persulfate dissolved in 1 M HCl to the mixture under vigorous mixing of the solvent. After polymerization, the product was centrifuged and washed three times with water and methanol. For obtaining EC300-CoED, untreated Ketjenblack is ultrasonically dispersed in 50 ml ethanol and an equal amount (to mass of Ketjenblack) of Co(II)-nitrate is added. Then in ethanol dissolved ethylenediamine is introduced and the mixture is boiled at 75 °C for 4 h under reflux before transferring it to a rotary evaporator for drying at 80 °C under vacuum. Both EC300-PA and EC300-CoED are pyrolyzed at 900 °C in an Ar atmosphere for 3 h after drying. In the case of EC300-CoED the transition metal residues are leached out by washing with 0.5 M H_2SO_4 and rinsing three times with ultrapure water.

In order to test the influence of ionomer impregnation, Nafion® was added to the carbon support and the Pt NP suspension. That is, Nafion® dissolved in acetone and mixed with the carbon before adding the NP suspension (EC300-NafA) or the Nafion®–acetone mixture was added to the EG-free NP suspension before mixing it with the carbon support (EC300-NafB). The ionomer content of the catalyst was 20 wt% in both cases.

2.4 Transmission electron microscopy (TEM)

The electrocatalysts were characterized by TEM using a Tecnai T20 G2 (Philips FEI, Oregon, USA) equipped with a thermionic electron gun operated at 200 eV. The micrographs were acquired using a Gatan 2K UltraScan 1000 CCD camera.

2.5 Small angle X-ray scattering (SAXS)

The platinum particle size distribution of the supported catalysts was determined by Small Angle X-ray Scattering (SAXS) using a SAXSLab instrument (JJ-X-ray, Denmark) equipped with a Rigaku 100 XL+ micro focus sealed X-ray tube and a Dectris 2D 300 K Pilatus detector. On this instrument the detector is moveable allowing different q-ranges to be accessed. Here the magnitude of the scattering vector is defined as $q = 4\pi/\lambda\sin(\theta)$ with λ being the X-ray wavelength and θ half of the scattering angle. Samples were sealed between two 5–7 μm thick mica windows and measurements were performed *in vacuo*. The data analysis follows[17] with small modifications. The scattering data are fitted to the following expression:

$$I(q) = C_1 I_{\mathrm{CARBON}}(q) + C_2 + C_3 \Pi(q) + C_4 \int P_{\mathrm{S}}(q,R)^2 D(R)\mathrm{d}R$$

where C_i are constants and the terms represent the background from the pure carbon support with no platinum loaded, a small constant background, a pore term given by the Lorentz expression:

$$\Pi(q) = \frac{a^4}{(1+a^2q^2)^2}$$

with a being a characteristic pore dimension and finally the sphere term representing the platinum NPs described by

a log-normal size distribution. The form factor amplitude of a sphere with radius R is given by:

$$P_S(q, R) = 4\pi R^3 \frac{\sin qR - qR\cos qR}{(qR)^3}$$

and the log-normal size distribution by:

$$D(R) = \frac{1}{R\sigma\sqrt{2\pi}} \exp\left(\frac{-[\ln(R/R_0)]^2}{2\sigma^2}\right)$$

where σ is the variance and R_0 the geometric mean of the log-normal distribution. The presented model fits are computed using home-written MATLAB code. The actual fits to the SAXS data are shown in Fig. S1 in ESI.†

2.6 Electrochemical characterization

The electrochemical measurements were performed using a computer controlled, home-built potentiostat and an All-Teflon cell[18] based on a three-compartment configuration using a rotating disk electrode (RDE) setup. The counter (auxiliary) electrode was a platinum mesh or carbon rod, the reference electrode a Schott Ag/AgCl/KCl(sat.) electrode placed in a separated compartment separated by an additional membrane (Nafion®) in order to avoid the diffusion of Cl^- ions into the main compartment.[19] All potentials in this work are referred to the reversible hydrogen electrode (RHE) potential, which was experimentally determined for each measurement series. All solutions were prepared in Millipore® water (>18.3 MΩ cm, TOC < 5 ppb). $HClO_4$ and HCl were from Merck (suprapur). The measurements were performed at room temperature. Prior to the RDE measurements the glassy carbon (GC) working electrode (5 mm diameter, 0.196 cm^2 geometrical surface area) was polished to mirror finish using alumina oxide paste, 0.3 and 0.05 μm (Buehler-Met, de-agglomerated α-alumina and γ-alumina, respectively), and cleaned ultrasonically in ultrapure water and cc. 70% $HClO_4$. The catalyst ink was prepared by mixing the catalyst powder with ultrapure water to a concentration of 0.14 m g_{Pt} cm^{-3} and ultrasonically dispersing the suspension for 30 min. Before applying the catalyst ink to the GC electrode the suspension was ultrasonically dispersed for an additional 5 minutes. Then a volume of 20 μL of the suspension was pipetted onto the GC electrode leading to a Pt loading of 14 μ g_{Pt} cm^{-2} and thereafter dried in a nitrogen gas stream. Care should be taken that the catalyst ink is not heated from the ultrasonic bath, to avoid errors from changing water density. Only samples with a uniform catalyst film, as controlled by eye, were analyzed. All electrochemical experiments were performed in 0.1 M $HClO_4$ solution. Prior to the measurements the electrolyte was de-aerated by purging with Ar gas (99.998%, Air Liquide), and the measurements were started with cleaning the catalyst by potential cycles between 0.05 and 1.1 V_{RHE} at a scan rate of 50 mV s^{-1}. The specific activity of the ORR was determined from the positive going RDE polarization curves recorded in O_2 saturated 0.1 M $HClO_4$ solution at a scan rate of 50 mV s^{-1} and at a rotation speed of 1600 rpm. The polarization curves were corrected for the non-faradaic background by subtracting the CVs recorded in Ar-purged electrolyte.[20] The solution resistance between the working electrode and the Luggin capillary was compensated for, resulting in an effective solution resistance of less than 3 Ω in each experiment. The electrochemically accessible surface area (ECSA) of the catalysts was determined from the CO stripping charge[21] recorded at a sweep rate of 50 mV s^{-1}.

3. Results and discussion

As outlined in the introduction, standard industrial synthesis protocols such as impregnation and precipitation inhibit systematic studies on supported fuel cell catalysts. Using a ligand free colloidal approach, we prepared a stock suspension of Pt NPs in EG. Then Pt NPs from the same stock suspension were supported on different HSA carbons. In Fig. 1 a series of 4 different such prepared catalysts is introduced. All catalysts were prepared to obtain a nominal Pt loading of 30 wt%. The supports are as-received EC300 carbon black, acid treated EC300 (EC300-HNO_3), EC300 mixed with Nafion® as well as Nafion® mixed to the NP suspension using as-received EC300 as a support (EC300-NafA and EC300-NafB). Representative TEM micrographs of the catalysts are shown along with their particle size distribution determined by SAXS. From the TEM micrographs it is seen that all four catalysts exhibit well distributed Pt NPs with defined particle size, thus demonstrating that the EG colloidal approach is an effective way to finely disperse metal NPs onto HSA carbon supports. However, comparing the micrographs of the catalysts to each other some differences are observed. The density of the Pt NPs on the untreated EC300 appears to be slightly lower as on the other supports and even some of the carbon flakes remained uncovered (not shown). At the same time very little NP agglomeration is observed.

In the literature, oxidation in nitric acid is reported to influence the metal particle–carbon surface interaction. Using traditional synthesis routes both beneficial[22,23] as well as negative[24,25] effects are reported. Under moderate conditions oxidation in nitric acid induces a more hydrophilic surface structure as well as a larger number of oxygen-containing functional groups (–COOH, –OH, –C═O) at the surface of the support.[26] These reports are consistent with our TEM results that confirm that the NP attachment is improved on EC300-HNO_3. Comparing the EC300 with the EC300-HNO_3 sample, the particle density on EC300-HNO_3 seems to be increased (see also ICP analysis below). However, at the same time some indications of NP agglomeration can be found (see highlighted particle agglomerates). As the micrographs are two-dimensional projections of three dimensional catalysts, we confirmed the agglomeration by an analysis of the particle size distribution established by SAXS. In the SAXS data it can be clearly seen that the average particle size for the EC300-HNO_3 sample is larger than for the EC300 sample. The average particle diameter increases from 1.7 ± 1.2 nm (FWHM taken as error), which is identical to the particle size of the Pt NPs in the stock solution, to 2.2 ± 1.4 nm.

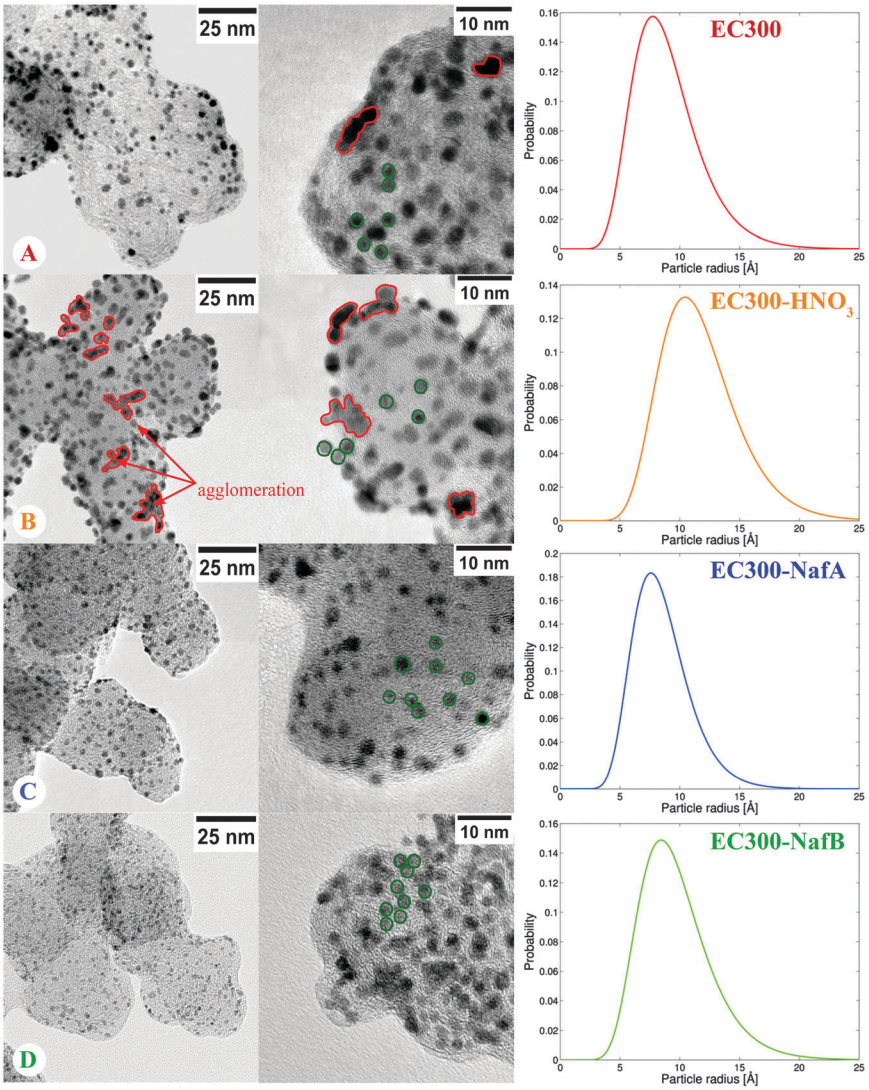

Fig. 1 TEM micrographs of synthesized catalysts at a low and high magnification in combination with their particle size distribution determined by SAXS. Pt NPs supported with nominal 30 wt% on (A) EC300, (B) EC300-HNO_3, (C) EC300-NafA, and (D) EC300-NafB. Some individual Pt NPs are marked by green circles, whereas red areas mark agglomerated NPs.

Addition of an ionomer to the catalyst results in an overall light grey background in the TEM micrographs, most likely because of additional electron scattering. Interestingly, in the TEM micrographs taken for an overview (left hand side of Fig. 1C and D) the Pt NPs appear to be smaller than for the other two samples (left hand side of Fig. 1A and B), whereas in the micrographs with higher resolution no significant difference in particle size is apparent. SAXS data reveal a better and instrument-independent insight over the particle size distribution than the TEM micrographs. The average particle size (diameter) of the EC300-NafA and EC300-NafB samples is 1.6 ± 1.0 and 1.8 ± 1.2 nm. Therefore, the apparent smaller particle sizes in the TEM overview micrographs are clearly an artifact due to the presence of the ionomer – an artifact that becomes less pronounced when zooming-in. Interestingly the average NP size of the EC300-NafB sample is slightly higher, which might be due to a Nafion film around the NPs.

Comparing TEM and SAXS results, it is demonstrated that although a TEM analysis is a useful visual tool for catalyst characterization, particle size distribution analyses based on TEM have some limitations. The limited contrast between the NPs and the support is one of the main difficulties in accurately assessing/estimating the exact particle size and its variance within the sample. Being a local method, even with careful TEM image analysis the difficult identification of the particle edge may lead to a significant over- or underestimation of particle size. A combination of TEM and SAXS, on the other hand, provides a complete picture of the structural properties of the catalysts both on local and overall scale.

As discussed above, the TEM micrographs in Fig. 1 indicate differences in Pt NP density between the catalysts in spite of the identical nominal value of 30 wt%. Therefore the actual Pt content of the catalysts was analyzed by ICP-MS after dissolving the catalyst in aqua regia. The results are shown in Fig. 2

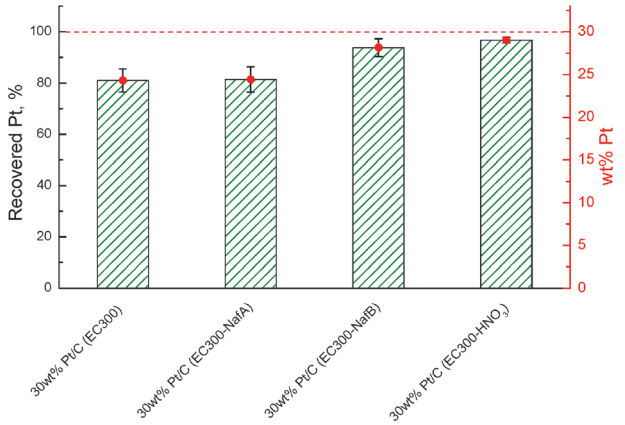

Fig. 2 Pt concentration in EC300, EC300-NafA, EC300-NafB, and EC300-HNO_3 samples determined by ICP-MS. The nominal (expected) Pt concentration calculated from the Pt NP suspension added to the carbon support is 30 wt%. On the left the axis indicates the percentage of Pt recovered from the expected concentration, the right hand sight axis indicates the absolute value of the Pt concentration.

confirming the impression from the TEM analysis. The Pt content of the EC300 and EC300-NafA samples is only 25 wt%, *i.e.* only 80% of the expected value. By contrast the Pt content of the EC300-NafB and EC300-HNO_3 samples is only slightly below the expected 30 wt%. This result reveals that for the EC300 and EC300-NafA samples a significant amount of Pt was lost during synthesis.

Before we discuss the particle attachment on the support further, we introduce the performance of the catalysts. The electrocatalytic performance of different Pt NP catalysts was determined using the rotating disc electrode (RDE) thin film methodology. The specific activity (I_s) of the oxygen reduction reaction (ORR) was measured at 0.9 V. From I_s and the ECSA, determined by CO stripping, the mass activity (I_m) was calculated. The results for a series of catalysts are summarized in Fig. 3. It is seen that for all catalysts I_s is higher than 500 μA cm_{Pt}^{-2}, except for two samples: Pt NPs supported on a nitrogen doped carbon prepared by aniline treatment (EC300-PA) and Pt NPs supported on a Nafion impregnated, nitrogen doped carbon sample (EC300-CoED-NafionB).

In the literature, reports of a substantial increase in the ORR activity can be found for nitrogen-doped Pt/C-ED and Pt/C-PA catalysts (as compared with nitrogen-free Pt/C). These reports are in contrast to our results where none of the treated nitrogen-doped samples showed significantly higher ORR activity. Instead some of the carbon treatments apparently result into problems with contaminations that inhibit the catalyst activity (see EC300-PA and EC300-CoED-NafionB).

The trend that functional groups result in enhanced particle sticking is also reflected in the values obtained for the ESCA. The Pt surface area varies between 44 ± 6 and 93 ± 6 m^2 g_{Pt}^{-1} as shown in Fig. 3. The lowest surface area is observed for a graphitized support, whereas the highest is obtained by ionomer impregnation according to method B. As the ICP analysis demonstrates, the variation in ECSA can partly be explained due to a loss of Pt NPs during preparation (all values are based on the amount of Pt used in the synthesis) and partly due to agglomeration during the synthesis (see SAXS results). Both acidic treatment and ionomer impregnation are found to be beneficial for increasing the ECSA as a result of enhanced particle sticking. By comparison the results concerning nitrogen-doping are somehow ambiguous. Whereas the EC300-CoED exhibited a significantly lower ECSA than the EC300 sample (but the same specific activity), EC300-PA exhibited a higher ECSA, but lower specific activity. Due to these inconclusive results we did not pursue the investigation of nitrogen-doped samples further in this study.

The increased particle sticking in the case of the acid treated carbon supports clearly indicates that the attachment (and distribution) of the Pt NPs is closely related to the surface functional groups of the carbon support. Graphitization, *i.e.* heat treatment of carbons under an inert atmosphere, results in desorption of the surface oxide groups. Therefore these types of low-oxide carbons have less anchoring sites for the attachment of metal nanoparticles thus favouring agglomeration. This is reflected by a decrease in the surface area of approximately 20% as compared with a standard support (EC300). Acid treatment of a carbon support results in an enhanced anchoring of Pt NPs to the support, but at the same time also promotes particle agglomeration during the colloidal synthesis even at moderate metal loading, *i.e.* this surface treatment comes at a cost.

In line with the uneven NP distribution, we therefore propose that on as-prepared EC300 oxygen-containing functional groups are unevenly distributed. This interpretation would explain a recent study of Pt NP degradation showing an inhomogeneous distribution of degradation channels in one and the same prepared Pt/C catalyst (using Vulcan XR72 as support),[9] indicating an inhomogeneous surface chemistry on HSA carbon supported catalysts. Ionomer impregnation is found to be the more favourable method to increase the anchoring of NPs onto the support. This is in agreement with reports that Nafion® can be used as an effective dispersant agent.[27,28] However, it should be also noted that different types of impregnation methods may largely influence the metal particle dispersion/utilization on the support material, as presented in a previous report[29] and our study.

O_2 reduction activities are also expressed in terms of A m g_{Pt}^{-1} ($I_{m(0.9\ V)}$ mass activity, see Fig. 3). As a consequence of the constant I_s, higher mass activities, >400 A g_{Pt}^{-1}, are obtained for the catalysts with higher Pt surface area, namely the catalysts with Nafion impregnated and acid treated carbons. This, however, is not due to a catalytic co-function, but simply due to better attachment of the Pt NPs to the support.

In order to compare the obtained performance data to standard commercial Pt/C catalysts we took a series of commercially available catalysts often used as a benchmark. The catalysts have a Pt nanoparticle size between 2–5 nm and a similar Pt loading of 40–50 wt%. For comparison we prepared an EC300 supported catalyst with the same Pt loading, *i.e.* 50 wt%.

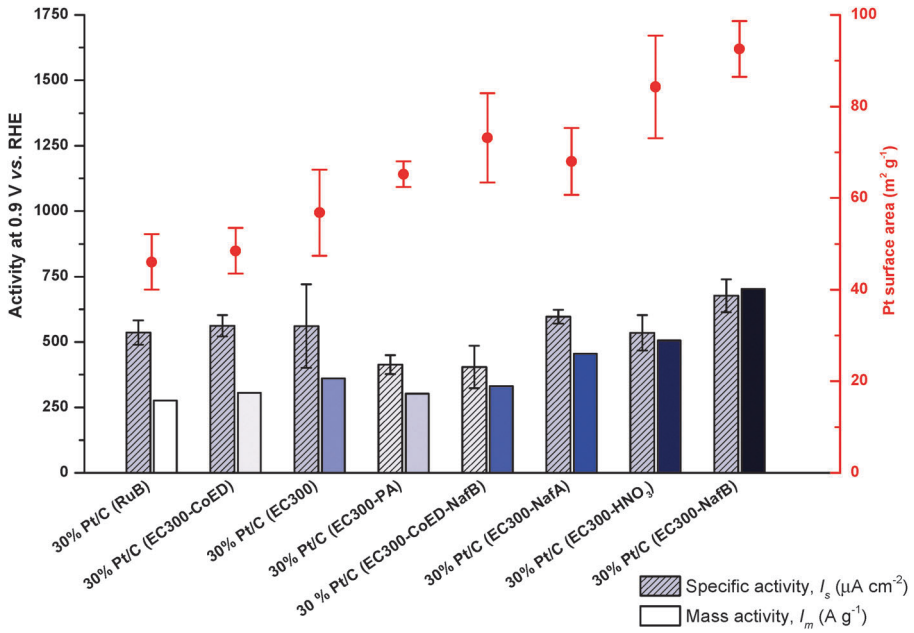

Fig. 3 Comparison of specific (I_s) and mass (I_m) activities of the model catalysts for ORR measured in oxygen saturated 0.1 M $HClO_4$ at 0.9 V *vs.* RHE and room temperature. Pt surface areas were determined from CO stripping. The mass activities were calculated from the respective specific activity and the surface area.

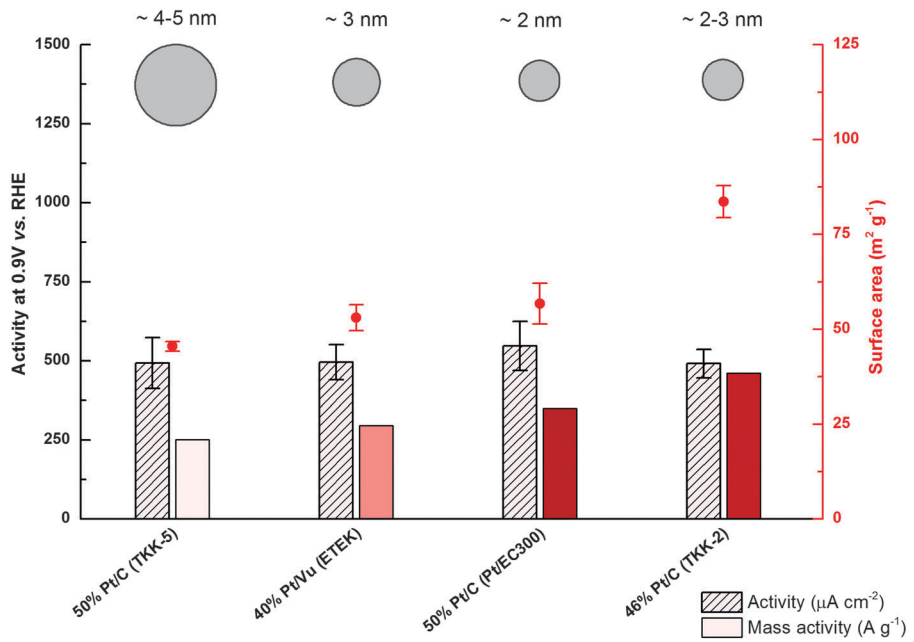

Fig. 4 Comparison of specific (I_s) and mass (I_m) activities of model catalysts for the ORR, measured in oxygen saturated 0.1 M $HClO_4$ at 0.9 V *vs.* RHE and room temperature. Pt surface areas were determined from CO stripping curves.

The results are summarized in Fig. 4. In agreement with our recent study on the particle size effect of Pt, the commercial and in-house prepared catalysts all have similar I_s, *i.e.* around 500 μA cm_{Pt}^{-2}, independent of support and particle size. In contrast to a predicted lower I_s,[30] our in-house prepared catalyst with a particle size of about 1.7 nm even has a slightly higher I_s than the TKK catalyst with 4–5 nm particle size. Therefore it can be concluded that neither the catalyst particle size nor the carbon support material is a key factor for the ORR activity in this particle size window (*ca.* 1.5–5 nm). In agreement with the particle size data, the experimentally determined ECSA of the catalysts varies between 45 ± 7 $m^2\ g^{-1}$ (50% TKK-5) and 84 ± 8 $m^2\ g^{-1}$ (46% TKK-2). As a consequence the mass activities increase in line and the commercial catalyst TKK-2 that has the highest surface area, with $I_{m(0.9\ V)} \sim 450\ A\ g^{-1}$, has the highest mass activity as well.

4. Conclusion

The colloidal synthesis approach employed for the preparation of well-defined electrocatalysts allows systematic studies of the influence of individual factors on the performance. An important feature of the synthesis is that no ligands or heat treatment of the catalysts are required. In the presented work we focused on the influence of different carbon supports, however studies employing non-carbon supports and different Pt based NPs are under preparation.

Concerning the carbon support, it is seen that for active catalysts, catalytic co-function of the support is negligible. The main function of the support is the effective anchoring of the NPs. If the support exhibits to little oxygen-containing functional groups and/or they are unevenly distributed, this effects an efficient dispersion of the catalysts. Particle anchoring can be promoted by HNO_3 treatment of the support. However, such harsh treatment also induces agglomeration and also might destabilize the carbon itself. Graphitization on the other hand stabilizes reportedly the carbon against corrosion,[8,31] however reduces considerably anchoring sites. This is not only valid for the employed synthesis strategy, but also may be the reason for larger particles and uneven particle distribution in commercial samples (especially after degradation tests) recently investigated in our group.[8] A more promising approach seems to be NP attachment by adding an ionomer to the NP suspension. As demonstrated, it favors a stable attachment of the Pt NPs onto the support without leading to agglomeration.

Acknowledgements

This work was supported by the Danish DFF through grant no. 10-081337 and the European Cost Action MP0903 Nanoalloys. We acknowledge the group of Dr Karl J. J. Mayrhofer at the MPIE for the ICP-MS analysis.

References

1 H. A. Gasteiger, S. S. Kocha, B. Sompalli and F. T. Wagner, *Appl. Catal., B*, 2005, **56**, 9–35.
2 H. A. Gasteiger and N. M. Marković, *Science*, 2009, **324**, 48–49.
3 J. Greeley, I. E. L. Stephens, A. S. Bondarenko, T. P. Johansson, H. A. Hansen, T. F. Jaramillo, J. Rossmeisl, I. Chorkendorff and J. K. Nørskov, *Nat. Chem.*, 2009, **1**, 552–556.
4 K. J. J. Mayrhofer and M. Arenz, *Nat. Chem.*, 2009, **1**, 518–519.
5 F. Jaouen, E. Proietti, M. Lefevre, R. Chenitz, J.-P. Dodelet, G. Wu, H. T. Chung, C. M. Johnston and P. Zelenay, *Energy Environ. Sci.*, 2011, **4**, 114–130.
6 Z. Yu, J. Zhang, Z. Liu, J. M. Ziegelbauer, H. Xin, I. Dutta, D. A. Muller and F. T. Wagner, *J. Phys. Chem. C*, 2012, **116**, 19877–19885.
7 K. J. J. Mayrhofer, J. C. Meier, S. J. Ashton, G. K. H. Wiberg, F. Kraus, M. Hanzlik and M. Arenz, *Electrochem. Commun.*, 2008, **10**, 1144–1147.
8 K. Schlogl, M. Hanzlik and M. Arenz, *J. Electrochem. Soc.*, 2012, **159**, B677–B682.
9 J. C. Meier, C. Galeano, I. Katsounaros, A. A. Topalov, A. Kostka, F. Schueth and K. J. J. Mayrhofer, *ACS Catal.*, 2012, **2**, 832–843.
10 P. L. Antonucci, V. Alderucci, N. Giordano, D. L. Cocke and H. Kim, *J. Appl. Electrochem.*, 1994, **24**, 58–65.
11 N. P. Subramanian, X. Li, V. Nallathambi, S. P. Kumaraguru, H. Colon-Mercado, G. Wu, J.-W. Lee and B. N. Popov, *J. Power Sources*, 2009, **188**, 38–44.
12 Y. Zhou, K. Neyerlin, T. S. Olson, S. Pylypenko, J. Bult, H. N. Dinh, T. Gennett, Z. Shao and R. O'Hayre, *Energy Environ. Sci.*, 2010, **3**, 1437–1446.
13 Y. Wang, J. W. Ren, K. Deng, L. L. Gui and Y. Q. Tang, *Chem. Mater.*, 2000, **12**, 1622–1627.
14 E. Antolini, *Appl. Catal., B*, 2009, **88**, 1–24.
15 Y. Guo, J. He, T. Wang, H. Xue, Y. Hu, G. Li, J. Tang and X. Sun, *J. Power Sources*, 2011, **196**, 9299–9307.
16 X. G. Li, S. Park and B. N. Popov, *J. Power Sources*, 2010, **195**, 445–452.
17 D. A. Stevens, S. Zhang, Z. Chen and J. R. Dahn, *Carbon*, 2003, **41**, 2769–2777.
18 K. J. J. Mayrhofer, G. K. H. Wiberg and M. Arenz, *J. Electrochem. Soc.*, 2008, **155**, P1–P5.
19 K. J. J. Mayrhofer, S. J. Ashton, J. Kreuzer and M. Arenz, *Int. J. Electrochem. Sci.*, 2009, **4**, 1–8.
20 M. Nesselberger, S. Ashton, J. C. Meier, I. Katsounaros, K. J. J. Mayrhofer and M. Arenz, *J. Am. Chem. Soc.*, 2011, **133**, 17428–17433.
21 H. A. Gasteiger, N. Markovic, P. N. Ross and E. J. Cairns, *J. Phys. Chem.*, 1994, **98**, 617–625.
22 G. C. Torres, E. L. Jablonski, G. T. Baronetti, A. A. Castro, S. R. deMiguel, O. A. Scelza, M. D. Blanco, M. A. P. Jimenez and J. L. G. Fierro, *Appl. Catal., A*, 1997, **161**, 213–226.
23 A. Guerrero-Ruiz, P. Badenes and I. Rodriguez-Ramos, *Appl. Catal., A*, 1998, **173**, 313–321.
24 F. Coloma, A. Sepulvedaescribano, J. L. G. Fierro and F. Rodriguezreinoso, *Langmuir*, 1994, **10**, 750–755.
25 D. J. Suh, T. J. Park and S. K. Ihm, *Carbon*, 1993, **31**, 427–435.
26 M. A. Fraga, E. Jordao, M. J. Mendes, M. M. A. Freitas, J. L. Faria and J. L. Figueiredo, *J. Catal.*, 2002, **209**, 355–364.
27 Z. G. Qi and A. Kaufman, *J. Power Sources*, 2003, **113**, 37–43.
28 E. A. Ticianelli, C. R. Derouin, A. Redondo and S. Srinivasan, *J. Electrochem. Soc.*, 1988, **135**, 2209–2214.
29 O. J. Curnick, B. G. Pollet and P. M. Mendes, *RSC Adv.*, 2012, **2**, 8368–8374.
30 K. Kinoshita, *J. Electrochem. Soc.*, 1990, **137**, 845–848.
31 P. V. Shanahan, L. Xu, C. Liang, M. Waje, S. Dai and Y. S. Yan, *J. Power Sources*, 2008, **185**, 423–427.

